Evidence of van Hove Singularities in Ordered Grain Boundaries of Graphene

Chuanxu Ma, Haifeng Sun, Yeliang Zhao, Bin Li, Qunxiang Li, Aidi Zhao, Xiaoping Wang, Yi Luo, Jinlong Yang, Bing Wang,* and J. G. Hou†

Hefei National Laboratory for Physical Sciences at the Microscale and Synergetic Innovation Center of Quantum Information & Quantum Physics, University of Science and Technology of China, Hefei, Anhui 230026, People's Republic of China

(Received 27 November 2013; revised manuscript received 16 March 2014; published 6 June 2014)

It has long been under debate whether the electron transport performance of graphene could be enhanced by the possible occurrence of van Hove singularities in grain boundaries. Here, we provide direct experimental evidence to confirm the existence of van Hove singularity states close to the Fermi energy in certain ordered grain boundaries using scanning tunneling microscopy. The intrinsic atomic and electronic structures of two ordered grain boundaries, one with alternative pentagon and heptagon rings and the other with alternative pentagon pair and octagon rings, are determined. It is firmly verified that the carrier concentration and, thus, the conductance around ordered grain boundaries can be significantly enhanced by the van Hove singularity states. This finding strongly suggests that a graphene nanoribbon with a properly embedded ordered grain boundary can be a promising structure to improve the performance of graphene-based electronic devices.

DOI: 10.1103/PhysRevLett.112.226802 PACS numbers: 73.22.Pr, 61.72.Mm, 68.37.Ef, 73.20.Hb

Grain boundaries (GBs) always exist in graphene grown by chemical vapor deposition [1–4], due to its polycrystalline nature [5,6]. There is growing interest in finding how the transport properties of graphene are related to their atomic and electronic structures for the sake of practical applications [7–11]. Although some efforts have been made by using transmission electron microscopy [12–14], or scanning tunneling microscopy (STM) or scanning tunneling spectroscopy (STS) [15–21], in most cases the characterized GBs were relatively disordered with a few exceptions [13,16]. As a quasi-one-dimensional (1D) structure, an ordered GB has a well-ordered linear periodic structure that contains pentagons, heptagons, and octagons. The density of states (DOS) of a 1D periodic structure is proportional to the inverse of the square root of the energy, which thus diverges close to band extrema, leading to the pronounced peaks close to the Fermi energy (E_F), called van Hove singularities (VHSs) [22]. The VHSs have been observed in nanotubes [23] and twisted bilayer graphenes [24–28]. Theoretical calculations have predicted the existence of VHSs in ordered GBs in single-layer graphenes [29–33]. However, the VHS states have not been experimentally verified in ordered GBs. The verification of VHS states of the ordered GBs in graphene has profound practical implications for many proposed electronic applications [7,8,34,35]. The possible VHS states can be an effective source to enrich the charge-carrier concentration around the GBs and, thus, to increase the electrical conductivity of graphene sheets and graphene nanoribbons (GNRs) [36,37]. Moreover, the determination of different electronic properties of ordered GBs from those of disordered GBs can be the key to understanding the existed contradictory results from transport measurements of individual GBs [38,39].

In this Letter, we give direct experimental evidence to verify the existence of VHS states in ordered GBs in a single-layer graphene on insulating SiO_2 substrate. The intrinsic electronic structures of two types of ordered GBs are well correlated to their atomically resolved structures using STM or STS joint with first-principles calculations. We find that the VHS states near the E_F show almost site-independent behaviors along the ordered GBs, in contrast to the site-dependent localized defect states in disordered GBs. Across the ordered GBs, a certain state slightly spreads into the nearby graphene sheet. Our findings help us understand the different transport properties of GBs and allow us to propose new structures by embedding GBs into GNRs for graphene-based electronic devices.

We prepared the single-layer graphene sample onto a 300 nm SiO_2/Si substrate, following the methods in Refs. [2,4]. The details for the sample preparation are described in the Supplemental Material [40]. The experimental measurements were carried out at 80 K. An electrochemical etched and well-cleaned tungsten tip was used. The dI/dV curves and maps were acquired using a lock-in preamplifier, with a typical sinusoidal modulation of 5–10 meV (rms) at 2000 Hz, and the sample bias with respect to the tip is adopted. Our calculations were carried out using density functional theory (DFT) with the projector-augmented wave method [42] as implemented in the Vienna ab initio simulation package (VASP) [43]. The generalized gradient approximation functional in the PBE form [44] was adopted to treat the exchange and correlation potential. All computational details can also be found in the Supplemental Material [40]. The STM images are simulated using a Tersoff and Hamanns formula [45] with a constant height of 3.0 Å.

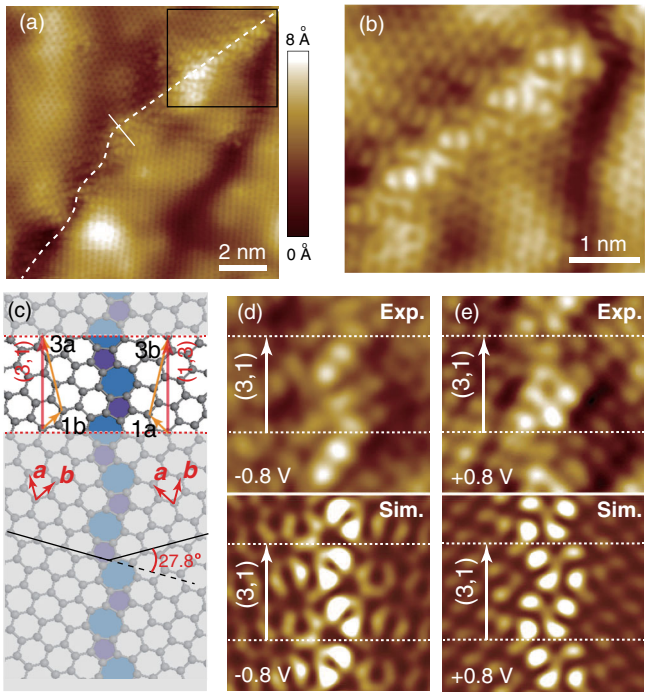

FIG. 1 (color online). (a) STM topographic image (11.5×11.5 nm^2), showing a GB in graphene and (b) magnified image of the marked area (5.8×5.2 nm^2, -0.8 V, and 0.5 nA). (c) Optimized structural model of the $(3,1)|(1,3)$ GB. The notation of the GB is shown. (d) Filled-state STM images (-0.8 V) and (e) empty-state STM images ($+0.8$ V) from experimental (upper, 1.8×1.7 nm^2) and simulated results (lower).

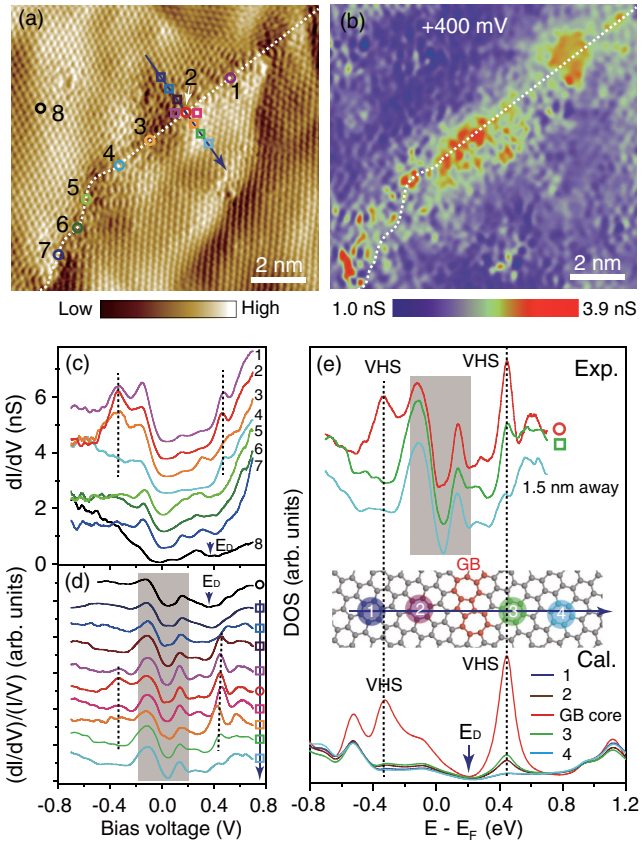

FIG. 2 (color online). (a) STM current image and (b) dI/dV map within the same area (11.2×10.4 nm^2, $+0.4$ V, and 0.5 nA). The dashed curves correspondingly mark the GB. (c) Representative dI/dV curves (-0.8 V and 0.5 nA) acquired along the GB (sites 1–7) and at sheet (site 8), marked by circles in (a). (d) $(dI/dV)/(I/V)$ curves acquired across the GB along the arrowed line in (a), shifted vertically for clarity. (e) Lower panel: calculated local DOSs. Upper panel: experimental data from (d) for comparison. Middle panel: model for calculations of the averaged local DOSs, which are obtained by summing the partial DOSs of the colored atoms and then averaging over the atom numbers. The dashed lines in (c)–(e) are eye guides only.

Figure 1(a) shows a STM topographic image of a GB between two grains, which tilt from each other by 28° (Supplemental Material Figure S1 [40]). The GB has a straight segment together with a curly segment. The image from the straight segment reveals a relatively ordered GB structure [Fig. 1(b)]. The structural information suggests a $(3,1)|(1,3)$ GB structure that consists of alternative pentagon and heptagon rings, as shown in Fig. 1(c). Here, the same notation as introduced in Ref. [29] is adopted. The optimized structure of $(3,1)|(1,3)$ GB gives a tilting angle of 27.8° between two grains, consistent with the experimental measurement. Moreover, the negative and positive bias STM images of the $(3,1)|(1,3)$ GB simulated at -0.8 and $+0.8$ V, shown in the lower panels of Figs. 1(d) and 1(e), respectively, well reproduce the main features of the experimental images and also agree with previous calculations [30].

Figures 2(a) and 2(b) give the current image and the dI/dV map ($+400$ mV) within the same area. Large tunneling conductance is observed along the GB (1 nm width), which is about 3 times higher than that on the graphene sheet. Such a feature is strikingly different from the ones obtained from the relatively disordered GBs (Supplemental Material Figs. S2 and S3 [40]). In disordered GBs, the tunneling conductance is at the similar level or even lower than that at the graphene sheet, confirming previous observations [17–19]. The dI/dV curves acquired at the ordered segment are quite different from those acquired at the curly segment and the sites away from the GB. Along the ordered segment [marked circles in Fig. 2(a)], there are distinct peaks locating at -330 and $+450$ meV [curves 1–3 in Fig. 2(c)], while they are invisible along the curly segment. The peak positions are almost site independent along the ordered GB, in contrast to the site-dependent features in disordered GBs. The latter is mainly a result from the localized defect states [17] (Supplemental Material Figs. S2 and S3 [40]). The Dirac point (E_D) is found to be located at $+350$ meV for the graphene sheet, indicating that the sheet itself should be a p-type doping. In Fig. 2(d), we give the normalized tunneling conductance curves $(dI/dV)/(I/V)$ for the sites

across the GB [squares in Fig. 2(a)]. The normalization (Supplemental Material Fig. S4 [40]) may help to minimize the voltage-dependent asymmetric feature in experimental data [17] and to allow comparison with the calculated local DOS. The peaks of −330 and +450 meV dominantly appear around the GB within 0.5 nm and are almost invisible at 1 nm on both sides of the GB [Fig. 2(d)]. In the shadowed region near the E_F, a gaplike feature seen at all sites could be assigned to the phonon-mediated inelastic mechanism proposed by Zhang *et al.* [46], which is not considered in our theoretical models.

The calculated local DOSs are plotted in the lower panel of Fig. 2(e). The GB core denotes the C atoms at defected region within a unit cell (the 16 red atoms in middle panel). The E_F of the calculated DOSs is set to −0.2 eV for a direct comparison with the experiments. It is seen that the separation of the calculated VHS peaks accords well with the experimental results. Moreover, the heights of the calculated VHS peaks show rapid decrease with the increase of the distance away from the GB (for sites 1–4 in the middle panel), especially for the filled state at −330 meV. This feature is also in good agreement with the experimental observations. Therefore, the occurrence of VHS states in such an ordered GB can be well established.

Another type of ordered GB is shown in Fig. 3(a). It gives quite symmetric patterns. The line profile along the GB center is also plotted in Fig. 3(a), showing a period of 0.5 nm. This structure can be assigned to a $(2,0)|(2,0)$ GB, which is supported by the experimental and simulated images in Figs. 3(b) and 3(c). This GB structure was observed in the graphene sample on a metal substrate [16] but has a quite different feature in comparison with our sample on SiO_2 substrate. The strong charge transfer between the graphene and the metal may already suppress the intrinsic GB properties. The experimental $(dI/dV)/(I/V)$ curves acquired at GB and at sheet (a site away from the GB by 5 nm) are shown in the upper panel of Fig. 3(d). Two prominent peaks located at −180 and +240 meV are observed at GB (red curve), in contrast to the feature at sheet (gray curve). To understand this behavior, we have calculated the local DOSs at different sites (middle panel), and the results are given in the lower panel of Fig. 3(d). Two peaks originated from VHS states, similar to the previous calculations [16,32], are observed in the GB core (red curve). The peak positions of the experiments are qualitatively in agreement with the calculated results. Note that the calculated peaks dramatically decrease with the increase of the distance from the GB core (green and blue curves). This behavior well resembles our experimental observations. Therefore, the experimental peaks can also be assigned to the VHS states. It is noticed that the GB length is only about 3.0 nm [Fig. 3(a)]. It may reasonably be attributed to the quantum confinement effect [47] for the difference in the peak separations between the experimental and theoretical results. Our calculations for the GB

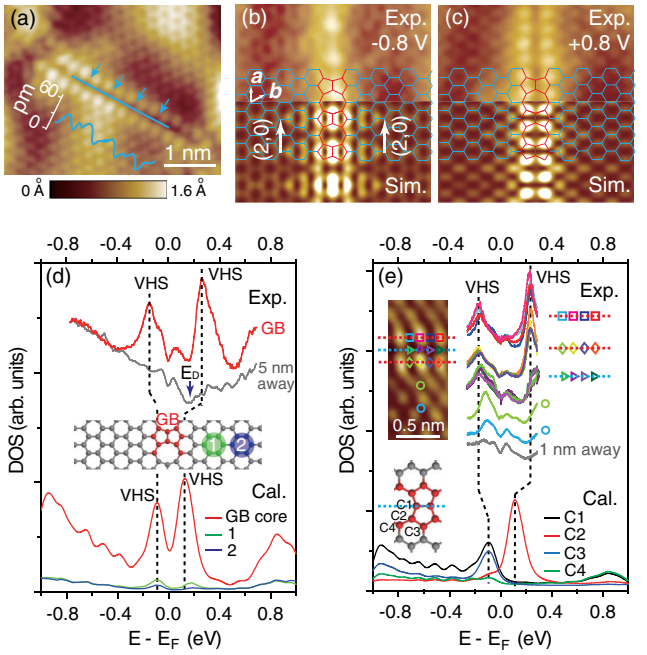

FIG. 3 (color online). (a) STM topographic image (4.2×3.3 nm^2, +0.8 V, and 0.5 nA) of a $(2,0)|(2,0)$ GB. The line profile shows a period of 0.5 nm along the GB (blue line). (b) Filled-state STM images (−0.8 V) and (c) empty-state STM images (+0.8 V) from experimental (upper, 2.9×1.4 nm^2) and simulated results (lower). The structural model of the $(2,0)|(2,0)$ GB is superposed. (d) Upper panel: an averaged $(dI/dV)/(I/V)$ curve at the GB and an individual $(dI/dV)/(I/V)$ curve at a site 5 nm from the GB. Lower panel: calculated DOSs at the labeled sites. Middle panel: model used in the calculations of the averaged local DOSs. (e) Upper panel: $(dI/dV)/(I/V)$ curves acquired at different sites (marked in upper-left inset), shifted for clarity. Lower panel: theoretically calculated partial DOSs of the four nonequivalent carbon atoms at GB core (marked in lower-left inset). The dashed lines in (d) and (e) are eyes guides only.

with different lengths provide an additional support (Supplemental Material Fig. S5 [40]), although the accuracy of DFT calculations in describing the VHS states of various GBs should be further examined.

The assignment of the peaks to the VHS states is supported by the atomically resolved local DOSs. As shown in the upper panel of Fig. 3(e) (Supplemental Material Fig. S6 [40]), two peaks at −180 and +240 meV are observed along the zigzag carbon chains of the GB (squares and diamonds), but a single peak at negative bias along the GB center (triangles). At sites away from the GB, the peak at the negative bias decreases with the increase of the distance and is still observable within 0.75 nm, accompanied with a peak shift toward E_F, but it totally disappears at 1.0 nm. These features can be well understood by the calculated partial DOSs in the lower panel of Fig. 3(e) and their spatial distributions [see below in Fig. 4(f)]. Our results indicate that the VHS empty states are mainly localized at the GB core, while the VHS filled states show somewhat delocalized nature.

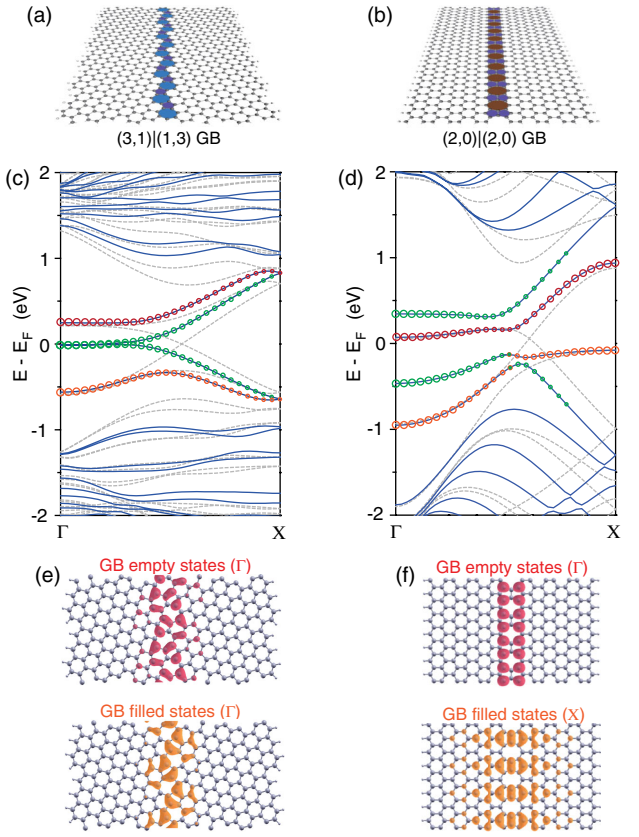

FIG. 4 (color online). [(a),(b)] Structural models, [(c),(d)] band structures (solid lines), and [(e),(f)] spatial distribution of GB states of (3,1)-GNR and (2,0)-GNR, respectively. The x direction is defined perpendicular to the GBs, and the y direction is parallel to the GBs. The (3,1)-GNR has partially zigzag edges, while (2,0)-GNR fully zigzag edges, with width of about 3.4 and 3.1 nm, respectively. The dashed lines in (c) and (d) give the band structures of graphene sheet containing $(3,1)|(1,3)$ GB and $(2,0)|(2,0)$ GB, respectively, for comparison. The open circles in (c) and (d) denote the contributions from the GB states (red: empty states, orange: filled states) and the edge states (green). The isosurface value is 0.01 e/Å^3 used in (e) and (f).

The finding of VHS states in GBs prompts us to design new types of graphene nanoribbons embedded with GB structures. Two types of nanoribbons containing $(3,1)|(1,3)$ GB and $(2,0)|(2,0)$ GB [Figs. 4(a) and 4(b)], abbreviated as (3,1)-GNR and (2,0)-GNR, respectively, are considered. Through the total energy calculations, we find that the ground states of (3,1)-GNR and (2,0)-GNR are nonmagnetic and antiferromagnetic (AFM) respectively. Their calculated band structures are shown in Figs. 4(c) and 4(d), and the spatial distribution of their VHS states at Γ or X point are plotted in Figs. 4(e) and 4(f), respectively. The VHS states in the GNRs with embedded GBs locate at almost the same energy positions as in graphene sheets with GBs. Their spatial distributions are mainly localized around the GBs, consistent with STM observations (Figs. 2 and 3), although the GB filled states of (2,0)-GNR are slightly delocalized. The states spread to the sheet by about 1.0 nm [Fig. 4(f)]. The (3,1)-GNR does not open up a gap due to the edge states at the E_F. Differently, the (2,0)-GNR is an AFM semiconductor that opens up an energy gap of about 0.20 eV between two VHS states near the E_F, similar to previous calculated results [31,48]. Interestingly, the gap between the edge states is about 0.42 eV, larger than the value of 0.29 eV for zigzag GNR of similar width [36]. The VHS states still survive when the width of (2,0)-GNR decreases to ~1.5 nm, i.e., only two six-membered C rings on both sides of the GBs.

An estimated carrier concentration of 6×10^{13} cm^{-2} is obtained from the calculated DOS for the $(2,0)|(2,0)$ GB [using the formula $n = \int_{E_D}^{E_F} g(E)dE$, where $g(E)$ is DOS], more than 1 order of magnitude higher than the value of 2.3×10^{12} cm^{-2} (estimated from the position of E_D [18,49]) at the sites far from the GB. A similar estimation for the $(3,1)|(1,3)$ GB gives a doubled carrier concentration, in agreement with our dI/dV map [Fig. 2(b)]. These results strongly indicate that GNRs with properly embedded GBs, say (2,0) GNR, can be new types of structures for fabricating electronic devices [4,7,50] with highly improved transport performance.

In previous transport measurements [38,39], the GBs were found to have either a detrimental effect or just slight impact on the transport properties of the graphene. This contradiction can, thus, be well explained by the presence of disordered or ordered GBs in different samples. The formation of ordered GBs with VHS states can improve the performance, whereas the disordered GBs could impede the electronic transport due to the increase of the electron scattering [39,51].

In summary, we experimentally determine the structures of two types of ordered GBs, i.e., $(3,1)|(1,3)$ GB and $(2,0)|(2,0)$ GB, in single-layer graphene on SiO_2/Si substrate. Their intrinsic electronic properties are well correlated to the atomically resolved structures. The existence of VHS states near the E_F value of the ordered GBs is verified. Our results indicate a new route to enhance the carrier concentration by embedding ordered GBs in graphene or GNRs, where the high carrier concentration is a desired property of graphene-based electronic devices.

This work was supported by National Key Basic Research Program (No. 2011CB921400, No. 2010CB923300, and No. 2014CB921101), by the Strategic Priority Research Program (B) of the CAS (No. XDB01020000), and the National Natural Science Foundation of China, by the USTC-HP HPC project, and by the SCCAS and Shanghai Supercomputer Center.

C. M. and H. S. contributed equally to this work.

*bwang@ustc.edu.cn
†jghou@ustc.edu.cn

[1] D. L. Duong *et al.*, Nature (London) **490**, 235 (2012).

[2] A. Reina, X. Jia, J. Ho, D. Nezich, H. Son, V. Bulovic, M. S. Dresselhaus, and J. Kong, Nano Lett. **9**, 30 (2009).
[3] K. S. Kim, Y. Zhao, H. Jang, S. Y. Lee, J. M. Kim, K. S. Kim, J.-H. Ahn, P. Kim, J.-Y. Choi, and B. H. Hong, Nature (London) **457**, 706 (2009).
[4] X. S. Li *et al.*, Science **324**, 1312 (2009).
[5] M. Kleman and J. Friedel, Rev. Mod. Phys. **80**, 61 (2008).
[6] L. P. Biró and P. Lambin, New J. Phys. **15**, 035024 (2013).
[7] A. K. Geim and K. S. Novoselov, Nat. Mater. **6**, 183 (2007).
[8] K. S. Novoselov, A. K. Geim, S. V. Morozov, D. Jiang, Y. Zhang, S. V. Dubonos, I. V. Grigorieva, and A. A. Firsov, Science **306**, 666 (2004).
[9] S. Das Sarma, S. Adam, E. H. Hwang, and E. Rossi, Rev. Mod. Phys. **83**, 407 (2011).
[10] A. H. Castro Neto, N. M. R. Peres, K. S. Novoselov, and A. K. Geim, Rev. Mod. Phys. **81**, 109 (2009).
[11] Z. Fei *et al.*, Nat. Nanotechnol. **8**, 821 (2013).
[12] P. Y. Huang *et al.*, Nature (London) **469**, 389 (2011).
[13] H. I. Rasool, C. Ophus, W. S. Klug, A. Zettl, and J. K. Gimzewski, Nat. Commun. **4**, 2811 (2013).
[14] K. Kim, Z. Lee, W. Regan, C. Kisielowski, M. F. Crommie, and A. Zettl, ACS Nano **5**, 2142 (2011).
[15] J. Červenka, M. I. Katsnelson, and C. F. J. Flipse, Nat. Phys. **5**, 840 (2009).
[16] J. Lahiri, Y. Lin, P. Bozkurt, I. I. Oleynik, and M. Batzill, Nat. Nanotechnol. **5**, 326 (2010).
[17] J. C. Koepke, J. D. Wood, D. Estrada, Z.-Y. Ong, K. T. He, E. Pop, and J. W. Lyding, ACS Nano **7**, 75 (2013).
[18] L. Tapasztó, P. Nemes-Incze, G. Dobrik, K. J. Yoo, C. Hwang, and L. P. Biró, Appl. Phys. Lett. **100**, 053114 (2012).
[19] K. W. Clark, X.-G. Zhang, I. V. Vlassiouk, G. He, R. M. Feenstra, and A.-P. Li, ACS Nano **7**, 7956 (2013).
[20] J. Coraux, A. T. N'Diaye, C. Busse, and T. Michely, Nano Lett. **8**, 565 (2008).
[21] P. Nemes-Incze, P. Vancsó, Z. Osváth, G. I. Márk, X. Jin, Y.-S. Kim, C. Hwang, P. Lambin, C. Chapelier, and L. PéterBiró, Carbon **64**, 178 (2013).
[22] L. van Hove, Phys. Rev. **89**, 1189 (1953).
[23] J.-C. Charlier, X. Blase, and S. Roche, Rev. Mod. Phys. **79**, 677 (2007).
[24] J. M. B. Lopes dos Santos, N. M. R. Peres, and A. H. Castro Neto, Phys. Rev. Lett. **99**, 256802 (2007).
[25] G. Li, A. Luican, J. M. B. Lopes dos Santos, A. H. Castro Neto, A. Reina, J. Kong, and E. Y. Andrei, Nat. Phys. **6**, 109 (2010).
[26] A. Luican, G. Li, A. Reina, J. Kong, R. R. Nair, K. S. Novoselov, A. K. Geim, and E. Y. Andrei, Phys. Rev. Lett. **106**, 126802 (2011).
[27] W. Yan, M. Liu, R.-F. Dou, L. Meng, L. Feng, Z.-D. Chu, Y. Zhang, Z. Liu, J.-C. Nie, and L. He, Phys. Rev. Lett. **109**, 126801 (2012).
[28] I. Brihuega, P. Mallet, H. González-Herrero, G. Trambly de Laissardière, M. M. Ugeda, L. Magaud, J. M. Gómez-Rodríguez, F. Ynduráin, and J.-Y. Veuillen, Phys. Rev. Lett. **109**, 196802 (2012).
[29] O. V. Yazyev and S. G. Louie, Nat. Mater. **9**, 806 (2010).
[30] O. V. Yazyev and S. G. Louie, Phys. Rev. B **81**, 195420 (2010).
[31] A. R. Botello-Méndez, X. Declerck, M. Terrones, H. Terrones, and J.-C. Charlier, Nanoscale **3**, 2868 (2011).
[32] S. S. Alexandre, A. D. Lúcio, A. H. Castro Neto, and R. W. Nunes, Nano Lett. **12**, 5097 (2012).
[33] D. Gunlycke and C. T. White, Phys. Rev. Lett. **106**, 136806 (2011).
[34] S. Bae, S. J. Kim, D. Shin, J.-H. Ahn, and B. H. Hong, Phys. Scr. **T146**, 014024 (2012).
[35] K. K. Kim, A. Reina, Y. Shi, H. Park, L.-J. Li, Y. H. Lee, and J. Kong, Nanotechnology **21**, 285205 (2010).
[36] Y.-W. Son, M. L. Cohen, and S. G. Louie, Nature (London) **444**, 347 (2006).
[37] X. Wang, X. Li, L. Zhang, Y. Yoon, P. K. Weber, H. Wang, J. Guo, and H. Dai, Science **324**, 768 (2009).
[38] A. W. Tsen, L. Brown, M. P. Levendorf, F. Ghahari, P. Y. Huang, R. W. Havener, C. S. Ruiz-Vargas, D. A. Muller, P. Kim, and J. Park, Science **336**, 1143 (2012).
[39] Q. K. Yu *et al.*, Nat. Mater. **10**, 443 (2011).
[40] See the Supplemental Material at http://link.aps.org/supplemental/10.1103/PhysRevLett.112.226802, which includes Ref. [41], for sample preparation and characterization, theoretical calculations, more STM images, STS spectra, and the detail of the analysis.
[41] N. N. Klimov, S. Jung, S. Zhu, T. Li, C. A. Wright, S. D. Solares, D. B. Newell, N. B. Zhitenev, and J. A. Stroscio, Science **336**, 1557 (2012).
[42] P. E. Blöchl, Phys. Rev. B **50**, 17953 (1994).
[43] G. Kresse and J. Hafner, Phys. Rev. B **47**, 558 (1993).
[44] J. P. Perdew, K. Burke, and M. Ernzerhof, Phys. Rev. Lett. **77**, 3865 (1996).
[45] J. Tersoff and D. R. Hamann, Phys. Rev. B **31**, 805 (1985).
[46] Y. Zhang, V. W. Brar, F. Wang, C. Girit, Y. Yayon, M. Panlasigui, A. Zettl, and M. F. Crommie, Nat. Phys. **4**, 627 (2008).
[47] T. W. Odom, J.-L. Huang, P. Kim, and C. M. Lieber, J. Phys. Chem. B **104**, 2794 (2000).
[48] Q. Q. Dai, Y. F. Zhu, and Q. Jiang, J. Phys. Chem. C **117**, 4791 (2013).
[49] L. Y. Zhao *et al.*, Science **333**, 999 (2011).
[50] M. Koch, F. Ample, C. Joachim, and L. Grill, Nat. Nanotechnol. **7**, 713 (2012).
[51] P. Vancsó, G. I. Márk, P. Lambin, A. Mayer, Y.-S. Kim, C. Hwang, and L. P. Biró, Carbon **64**, 101 (2013).